MFN= 007132
01 SID/SCD
02 5719
03 INPE-5719-PRE/1881
04 CEA
05 S
06 as
10 Takahashi, Hisao
10 Clemesha, Barclay Robert
10 Sahai, Yogeshwar
10 Batista, Paulo Prado
10 Simonich, Dale Martin
12 Seasonal variations of mesospheric hydrogen and ozone concentrations derived from ground-based airglow and lidar observations
14 5987-5993
30 Journal of Geophysical Research
31 97
32 D5
40 En
41 En
42 <E>
58 DAE
61 <PI>
64 Apr. <1992>
68 PRE
76 AERONOMIA
83 Upper atmospheric airglow emissions in the mesopause region, OI557.7 nm, NaD at 589.3 nm and OH(9,4) band at 774.6 nm have been observed since 1977 at Cachoeira Paulista (22.7 degrees S, 45.0 degrees W), Brazil. The seasonal dependence of the intensity variations of these emissions was studied using the data from a total of 560 nights, during the period June 1977 to November 1986. Strong semiannual variations in the NaD and OI557.7 nm emissions were observed with maxima at the equinoxes, in contrast to the OH(9,4) emission, which showed a much smaller seasonal variation. Hydrogen and ozone concentrations at around 87-89 km were calculated using the observed NaD and OH(9,4) band intensities and the sodium concentration observed by lidar at a nearby station. The obtained seasonal variations of the two species, opposite in phase with each other, are in good agreement with current atmospheric dynamics models, which show a seasonal variation of the vertical transport of atomic oxygen and hydrogen.
90 b
91 FDB-19960313
92 FDB-MLR

JOURNAL OF GEOPHYSICAL RESEARCH, VOL. 97, NO. D5, PAGES 5987-5993, APRIL 20, 1992

Seasonal Variations of Mesospheric Hydrogen and Ozone Concentrations Derived From Ground-Based Airglow and Lidar Observations

H. TAKAHASHI, B. R. CLEMESHA, Y. SAHAI, P. P. BATISTA AND D. M. SIMONICH

Instituto Nacional de Pesquisas Espaciais, São José dos Campos, São Paulo, Brazil

Upper atmospheric airglow emissions in the mesopause region, OI557.7 nm, NaD at 589.3 nm and OII(9,4) band at 771.6 nm have been observed since 1977 at Cachoeira Paulista (22.7°S, 45.0°W), Brazil. The seasonal dependence of the intensity variations of these emissions was studied using the data from a total of 560 nights, during the period June 1977 to November 1986. Strong semiannual variations in the NaD and OI557.7 nm emissions were observed with maxima at the equinoxes, in contrast to the OH(9,4) emission, which showed a much smaller seasonal variation. Hydrogen and ozone concentrations at around 87-89 km were calculated using the observed NaD and OH(9,4) band intensities and the sodium concentration observed by lidar at a nearby station. The obtained seasonal variations of the two species, opposite in phase with each other, are in good agreement with current atmospheric dynamics models, which show a seasonal variation of the vertical transport of atomic oxygen and hydrogen.

1. INTRODUCTION

Day-to-day and seasonal variations of the upper mesospheric airglow emission intensities, atomic oxygen at 557.7 nm (hereafter OI5577), NaD at 589.3 nm (hereafter NaD) and OII(9,4) band at 775.0 nm (hereafter OII(9,4)) are mainly controlled by the atomic oxygen, ozone and atomic hydrogen concentrations in the mesopause region. These minor constituents, in turn, are controlled by solar radiation flux, vertical mixing and horizontal transport processes. In their atmospheric model, *Garcia and Solomon* [1985] showed seasonal variations of dynamical processes which are strong in summer and winter but weak in the equinox seasons and which should affect the concentrations of minor species in the mesopause region. Recent satellite observations of mesospheric ozone by *Thomas* [1990a] revealed a clear seasonal dependence. *Le Texier et al.* [1987] presented seasonal variations of OII airglow intensity derived from their model calculations, which took into account the seasonal variation of the dynamical mixing process. They showed that the OII intensities are controlled by the atomic oxygen mixing ratio in the mesopause region. They also studied the seasonal variation of the hydrogen and ozone concentrations. These calculations suggest the possibility of using the airglow data to estimate minor constituent concentrations and, in turn, of studying the dynamical processes occurring in the mesopause region.

The ground-based airglow data, published previously, have been used to study nocturnal, diurnal, seasonal and long term variations of emission intensities [e.g., *Wiens and Weill*, 1973; *Takahashi et al.*, 1984]. Correlations between the intensities have also been studied by many workers [e.g., *Takahashi et al.*, 1979; *Takeuchi et al.*, 1981; *Rodrigo et al.*, 1985]. However, there have been few attempts to use these ground-based observational data to estimate the minor constituent concentrations at the emission heights. In the last decade, a number of rocket observations have been carried out with the purpose of obtaining the atomic oxygen concentration in the 85 to 110 km region, using the oxygen resonance lamp technique [*Dickinson et al.*, 1980], and the OI5577 and O_2 atmospheric band emission profiles [*Witt et al.*, 1979; *Murtagh et al.*, 1990]. The OII emission profile observed by rocket has also been used to estimate the atomic oxygen concentration in the 80 to 100 km region by *Good* [1976]. *Ulwick et al.* [1987] determined the hydrogen concentration from simultaneous rocket observation of the O_2 infrared 1.27 μm and OII emissions. Using ground-based observations, *Kirchhoff et al.* [1981] estimated the ozone density using simultaneous lidar measurements of the sodium density profile and photometric measurements of the sodium nightglow intensity.

The purpose of the present paper is to investigate the seasonal variation of the mesospheric airglow emissions, OI5577, NaD and OII(9,4) band, using the data obtained from the Cachoeira Paulista airglow observatory during almost 10 years. Also, using the observed nocturnal mean values of the NaD and OII(9,4) emissions, together with the Na abundance observed by lidar, the hydrogen and ozone concentrations in the emission layer height were calculated. This is, as far as we know, the first attempt to estimate both the hydrogen and ozone concentrations using simultaneous airglow and lidar observations.

2. OBSERVATIONS

Simultaneous measurements of the mesospheric airglow emissions, OI5577, NaD and OII(9,4) band, and the OII rotational temperature have been carried out at Cachoeira Paulista (22.7°S, 45.0°W) since 1976. A multichannel tilting filter type photometer was used for all observations. The photometer characteristics and the calibration procedure adopted have been described elsewhere [*Takahashi and Batista*, 1981]. The data used in the present work are from June 1977 to November 1986, a total of 560 nights of observation. This period includes the solar maximum in 1979 and the solar minimum period in 1986. The airglow data showed a long-term variation correlated to solar activity [*Takahashi*

Paper number 91JD03015.
0148-0227/92/91JD-03015$05.00

et al., 1984]. The emphasis in the present study, however, is on the seasonal dependence of the emissions.

Sodium abundance between 80 to 100 km of altitude was measured by a lidar operated at São José dos Campos (23.2°S, 45.9°W), about 100 km from the airglow observatory. The general features of the sodium profile observed at this site have been published elsewhere [*Simonich et al.*, 1979]. In the present study, the sodium abundance data taken from 1972 to 1986, with a total of 710 days of observation, were used.

3. Seasonal Variation of the Mesospheric Airglow

Nocturnal mean values of the OI5577, NaD and OII(9,4) band intensities, obtained from a total of 560 nights from June 1977 to November 1986, are plotted against annual day number in Figures 1, 2 and 3. Only nights with more than 5 hours of observation were used in this study. Each point in the figures corresponds to one night. No correction was made for long-term trends (most probably the solar cycle effect). Also shown in the figures are the monthly means of the emissions.

It is clear from Figures 1 and 2 that the OI5577 and NaD emissions show strong semiannual variations with maxima in May and November-December, in the case of OI5577, and May and October in the case of NaD. In the case of the OH(9,4) emission, in Figure 3, a similar semiannual tendency can be seen, but the amplitude of oscillation is significantly less. The annual component peaks in November.

In order to determine the phase and amplitude of the annual and semiannual components of these mesospheric parameters, the following model was fitted to all data sets in the least mean square sense:

$$Y = A_0 + A_1 cos\{(2\pi/365)(t - f_1)\} + A_2 cos\{(2\pi/182.5)(t - f_2)\}$$

where A_0 is the annual mean, and A_1 and A_2, and f_1 and f_2 are the amplitudes and phases of the annual and semiannual components, respectively. The obtained individual components are listed in Table 1. As expected, from Figure 2, the amplitude of the semi-annual component of the NaD emission is the largest, 60% of the annual mean A_0. The OI5577 annual component is significant, 20% of A_0, although the semiannual component is dominant, 30% of A_0. In the case of the OII(9,4) band intensities, the annual and semiannual components have about the same, small amplitude, around 5% of A_0. For both OI5577 and NaD the semiannual component peaks in April and October, for OII(9,4) it peaks in May and November. The annual component has its maximum in summer for OI5577 and OH(9,4), and in winter for NaD.

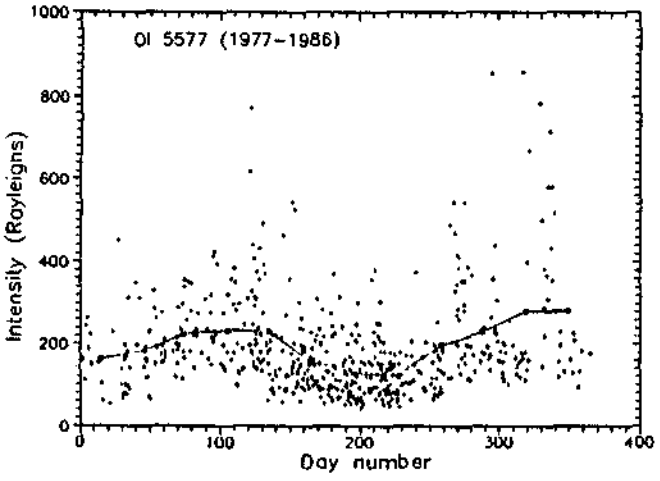

Fig. 1. Nocturnal mean values of the OI 557.7 nm emission intensity as a function of the day number (plotted) and the monthly mean values (solid line).

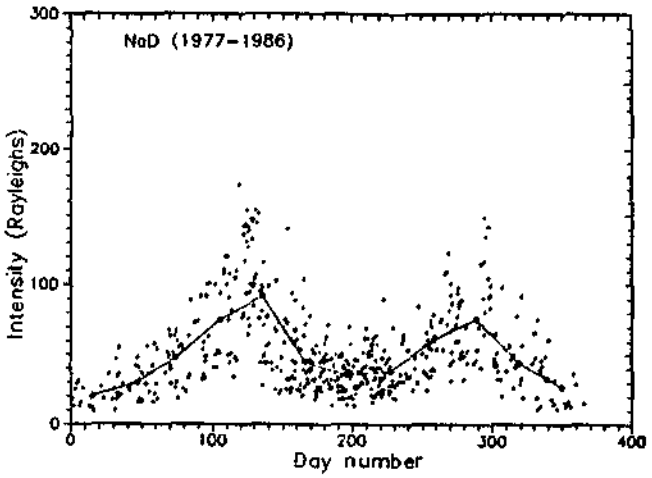

Fig. 2. Same as Figure 1, but for the NaD emission.

4. Discussion

4.1. Seasonal Effects in the Mesospheric Emissions

OI557.7 nm emission. The production process for excited $O(^1S)$, which is responsible for the OI5577 green line emission in the lower thermosphere, is believed to be through a two-step energy transfer process (see, for example, *Bates* [1988]):

$$O + O + M \rightarrow O_2^* + M,$$

$$O_2^* + O \rightarrow O_2 + O(^1S)$$

so that the volume emission rate is directly related to the atomic oxygen concentration at the emission height. From rocket observations [e.g., *McDade et al.*, 1986] the peak emis-

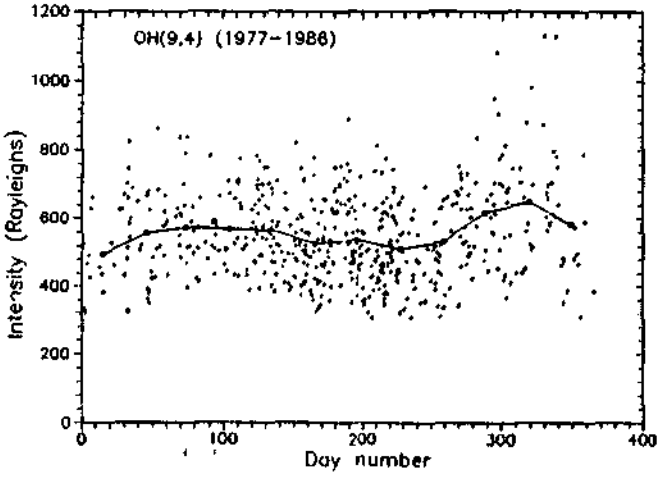

Fig. 3. Same as Figure 1, but for the OII(9,4) band intensity.

TABLE 1. Annual and Semiannual Oscillation Components of the Mesospheric Airglow Emission Intensities

		Annual		Semiannual	
Emission	A_0, R	A_1, R	f_1, d	A_2, R	f_2, d
OI 5577	206	39.3	360	59.9	117
NaD	50	13.0	170	30.1	109
OH(9,4)	558	27.7	3	32.0	135

R: rayleighs, d: day number.

sion height is located at around hmax = 97±3 km, where the atomic oxygen has its peak density. Therefore, the day-to-day and seasonal variations of the OI5577 intensity observed from the ground provide a good indicator of the atomic oxygen variation at around 95 to 100 km. We assume now that the OI5577 column intensity is roughly proportional to:

$$I_{5577} \propto [O]^2[M]$$

where we have adopted *McDade et al.*'s [1986] argument, i.e., the main quenching agent of the $O(^1S)$ precursor should be atomic oxygen and the quantum radiation is the main loss process of $O(^1S)$. In this case, the increase of more than a factor of 2 from winter (July) to spring (October) visible in Figure 1, corresponds to a 43% variation in the atomic oxygen density at around 97 km. This value is smaller than that which *Garcia and Solomon* [1985] predicted in their model, which is about 80%.

NaD 589.3 nm emission. The nightglow NaD_1 and D_2 emissions are produced in the following aeronomic reactions:

$$Na + O_3 \rightarrow NaO + O_2 \quad k_1 \qquad (1)$$

$$NaO + O \rightarrow Na(^2P) + O_2 \quad a, k_2 \qquad (2)$$

$$Na(^2P) \rightarrow Na + h\nu(589.0, 589.6\ nm) \qquad (3)$$

where k_1 and k_2 represent the reaction rates in the usual manner and a represents the fraction of sodium left in the excited ^2P state.

The reactions (1) and (2) are in photochemical equilibrium in the mesopause region, so that the volume emission rate of NaD can be expressed as:

$$V_{NaD} = ak_1[Na][O_3] \qquad (4)$$

It is known from rocket observations [*Greer and Best*, 1967; *Stegman and Witt*, 1977] that the NaD emission height is located at around 89 km. Therefore, if one knows the sodium concentration, the ozone concentrations at around 89 km can be calculated by measuring V_{NaD}. The sodium abundance observed from São José dos Campos, as will be discussed later, shows moderate annual variation, a broad maximum in late winter (July and August) and minimum in summer (December and January). Therefore, the strong equinox maxima observed in the sodium nightglow should be due to the variation of ozone concentration at around 89 km.

OH(9,4) band emission. The chemical reaction between hydrogen and ozone in the mesopause region:

$$H + O_3 \rightarrow OH(v = 9,8,7) + O_2 \quad k_5 \qquad (5)$$

is responsible for the production of excited OH in the vibrational levels $v = 9, 8$ and 7 [*Bates and Nicolet*, 1950]. The excited OH molecules are deactivated in the following processes:

$$OH(9) + M \rightarrow OH(v < 9) + M \quad k_6 \qquad (6)$$

$$OH(9) + O \rightarrow O_2^* + H \quad k_7 \qquad (7)$$

$$OH(9) \rightarrow OH(v < 9) + h\nu \quad A_9, A_{94} \qquad (8)$$

where M represents O_2 and N_2, and A_9 and A_{94} are vibrational transition probabilities. The OH(9,4) volume intensity is, therefore,

$$V_{OH94} = \frac{A_{94}k_5 f(9)[H][O_3]}{A_9 + k_6[M] + k_7[O]} \qquad (9)$$

where $f(9)$ is a quantum yield producing $OH(v = 9)$ in (5).

In the region of the OH emission layer between 80 to 100 km, the ozone production process:

$$O + O_2 + M \rightarrow O_3 + M \qquad (10)$$

and (5) are in photochemical equilibrium.

The V_{OH94} is, therefore, proportional to the ozone production rate, i.e,

$$V_{OH94} \propto [O][O_2][M] \qquad (11)$$

In other words, the OH emission intensity is proportional to the atomic oxygen density in the region of the peak of the emission layer. According to *Baker and Stair* [1988] this is located at 87±2 km. The small amplitude of the seasonal variation of the OH emission intensity indicates that at this height atomic oxygen varies little. At first sight this seems to be inconsistent with the observed seasonal variation in NaD, which shows strong equinoctial peaks, indicating the existence of strong equinoctial maxima in ozone concentration. It must be remembered, however, that the ozone equilibrium in the mesopause region is given by

$$[O_3] \propto \frac{[O][O_2][M]}{[H]}$$

so the implication of these observations is that H must have a seasonal variation opposite to that of O_3.

The small observed seasonal variation in the OH emission intensity at low latitudes has been discussed by *Le Texier et al.* [1987]. These workers used a two-dimensional dynamical- photochemical model which included the effects of advection produced by the mean meridional circulation, and vertical eddy diffusion produced by the breaking of gravity waves. For low latitudes their model predicts a semiannual variation, with an amplitude of about 10%, giving maximum intensities in April and October. Our present data are in reasonable agreement with the model calculation of Le Texier et al., except for the sharp peak which we observe in November, not predicted by the model.

The annual components of the seasonal variations observed in OI5577 and OH at our latitude indicate that the atomic oxygen concentration above 85 km increases in summer. Although this could be the result of changes in eddy diffusion, as discussed later, we believe that it is more likely to be the result of vertical advection associated with the meridional circulation. Our results are consistent with *Cog-*

ger et al. [1981], who suggested a sectorial meridional circulation pattern in addition to the global summer to winter cell. A realistic atmospheric model, including a detailed wind system, would be necessary to carry the present discussion further.

4.2. Ozone and Hydrogen Concentration

Since the intensities of the NaD and OII emissions depend on the local ozone and hydrogen atom concentrations, it is possible, introducing certain assumptions, to use our observations to estimate the seasonal variations in these constituents.

Ozone concentration at 89 Km. Using (4), the NaD emission column intensity can be expressed as

$$I_{NaD} = ak_1 \int_{80}^{120} [Na][O_3]\, dz \quad photons/cm^2\ column \tag{12}$$

Our lidar profiles of sodium have a 1 km height resolution, so we replace the integral of (12) with a summation. We also normalize the Na and O_3 profiles at 89 km, where the NaD emission should be maximum, resulting in

$$I_{NaD} = ak_1[Na]_{89}[O_3]_{89}.10^5 \sum_{n=1}^{40} \{p_n(Na)p_n(O_3)\}$$

where $p_n(Na)$ and $p_n(O_3)$ are normalized profiles, unity at 89 km, and $[Na]_{89}$ and $[O_3]_{89}$ represent concentration in cm^{-3}, at 89 km.

Therefore the O_3 concentration can be expressed as:

$$[O_3]_{89} = \frac{10^{-5} I_{NaD}}{ak_1[Na]_{89}} \left[\sum_{n=1}^{40} \{p_n(Na)p_n(O_3)\}\right]^{-1} \tag{13}$$

The reaction rate k_1 and the fraction a adopted in this work are listed in Table 2. There is uncertainty about the fraction a [*Plane and Husain*, 1986]. In this work the value presented by *Bates and Ojha* [1980] was used.

In order to calculate $[O_3]$ at 89 km, the relative Na and O_3 profiles must be assumed. Since the airglow observation and Na lidar measurement were not always carried out simultaneously, we used an average Na profile for our station. Monthly averaged total abundances were used to obtain the values $[Na]_{89}$. The adopted [Na] profile and the seasonal variation of the total Na abundance are shown in Figure 4. It should be pointed out that the Na abundance shows a seasonal variation which is predominantly annual, with maximum abundance occurring in winter. This is quite different to the NaD airglow emission variation which, as described above, is mainly semiannual. The effects of the day-to-day and seasonal variations of the [Na] profile on the evaluation of (13) will be discussed in the next section of this report.

Few rocket measurements of the nighttime ozone profile have been carried out. Published results are listed in Table 3. In order to evaluate the possible effects of the variability in the ozone profile we have used each of the profiles in turn to compute the summation of (13), resulting in:

$$\sum_{n=1}^{40} \{p_n(Na)p_n(O_3)\} = 10.6 \pm 2.0 \tag{14}$$

The error range shown is due to the variability of these adopted ozone profiles. Putting the summation factor (14) into (13),

$$[O_3]_{89} = 5.47(\pm 0.9)10^9 \frac{R_{NaD}}{[Na]_{89}} \tag{15}$$

where R_{NaD} represents the NaD intensity in rayleighs. The results are shown in Figure 5. Each plot corresponds to a nocturnal mean ozone concentration at 89 km. Also shown are the monthly averaged values (solid line). Strong seasonal variations with maxima at the end of April and the middle of October are evident. This agrees quite well with satellite observations [*Thomas*, 1990a]. However the variation of ±50% (5×10^7 to 1.5×10^8 cm^{-3}) about the annual mean is significantly larger than that found by Thomas, which was about ±20%.

Hydrogen concentration at 87 Km. The hydrogen concentration at around 87 km can be determined from $[O_3]$ obtained in the previous section and the observed OII(9,4) column emission rate:

$$I_{OH(9,4)} = \int_{80}^{120} \frac{A_{94}k_5 f(9)[H][O_3]}{A_9(1 + (k_6/A_9)[O_2])}\, dz \tag{16}$$

Since the quenching of OII(9) by O and N_2 in (9) is small compared to that by O_2 (*McDade et al.*, 1987), they were neglected. The hydrogen and ozone height profiles are normalized at 87 km where the OII emission has a peak intensity. Integrating (16) with a height interval of 1 km gives:

$$I_{OH(9,4)} = (A_{94}/A_9)k_5 f(9)[H]_{87}[O_3]_{87}10^5 \times \sum_{n=1}^{40} \frac{p_n(H)p_n(O_3)}{1 + (k_6/A_9)[O_2]_n} \tag{17}$$

where $[O_2]_n$ is the O_2 concentration adopted with a height interval of 1 km, $p_n(H)$ and $p_n(O_3)$ are profiles normalized to unity at 87 km, and $[H]_{87}$ and $[O_3]_{87}$ represent concentration in cm^{-3} at 87 km. The constants used in the calculation are listed in Table 2. The $[O_2]$ profile was taken from MSIS 86 by *Hedin* [1987] for equinox conditions at our latitude. The hydrogen and ozone profiles for nighttime conditions were chosen from recent rocket observations and model calculations listed in Table 3. The result of the summation is

TABLE 2. Adopted Rate Coefficients and Constants

Reaction	Coefficient	Range	Reference
(1)	$k_1 = 1.6\times10^{-9}\exp(-195/T)$	$3\sim7\times10^{-10}$	*Worsnop et al.* [1991]
(2)	$a = 0.3$	$0.01 \sim 0.3$	*Bates and Ojha* [1980]
(5)	$k_5 = 1.47\times10^{-10}\exp(-496/T)$	$1\sim3\times10^{-11}$	*Keyser*[1979]
(6)	$k_{6,O_2}/A_9 = 5.3\times10^{-14}$	$5.3\sim14\times10^{-14}$	*McDade et al.* [1987]
(7)	$k_{7,O} = 0$	—	*McDade et al.* [1987]
(8)	$A_{94}/A_9 = 4.84\times10^{-3}$	$3.9\sim14.7\times10^{-3}$	*Murphy* [1971]
(9)	$f(9) = 0.53$	$0.3 \sim 0.6$	*Takahashi and Batista* [1981]

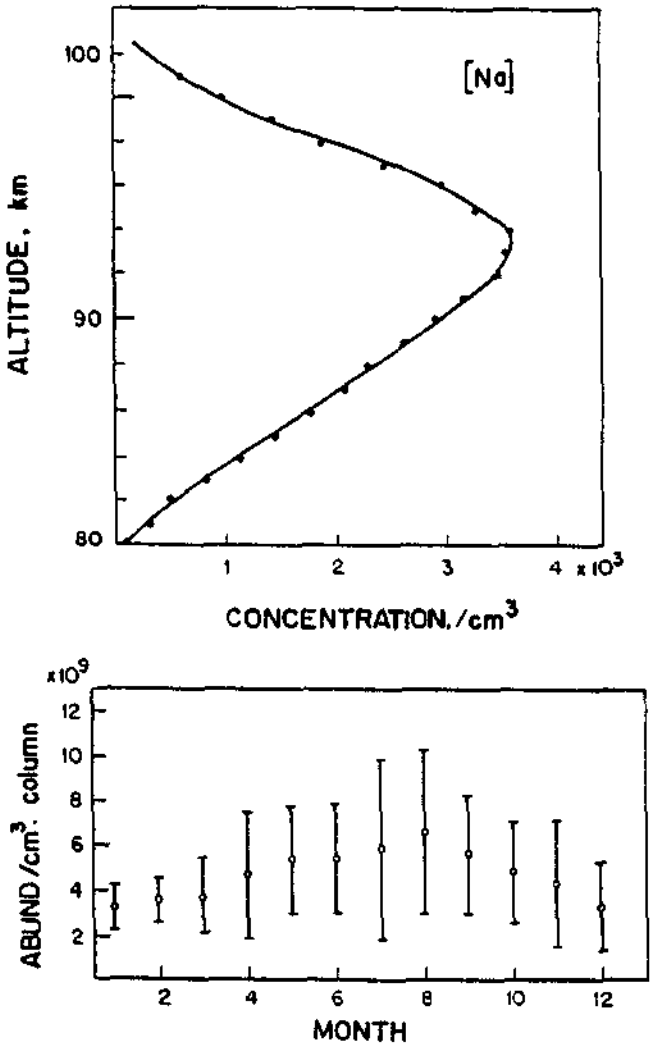

Fig. 4. (Top)Observed mean sodium density profile. (Botton) The seasonal variation of the total abundance.

$$\sum_{n=1}^{40} \frac{p_n(\mathrm{H})p_n(\mathrm{O_3})}{1 + (k_6/A_9)[\mathrm{O_2}]_n} = 5.01 \pm 0.76 \qquad (18)$$

where the expressed error range is from the different combinations of $p(\mathrm{H})$ and $p(\mathrm{O_3})$ used. Substituting (18) into (17) gives

$$[\mathrm{H}]_{87} = 6.14(\pm 1.0)10^{13}\frac{R_{\mathrm{OH}94}}{[\mathrm{O_3}]_{87}} \qquad (19)$$

where $R_{\mathrm{OH}94}$ is expressed in rayleighs.

In this calculation, the ozone density at 89 km obtained from (15) was used as $[\mathrm{O_3}]_{87}$. Since the ozone concentration has a secondary peak around 88 km and its gradient with height is small in this height region this should introduce only a small error. The error range of (19) is mainly dependent on the adopted $p(\mathrm{H})$ and $p(\mathrm{O_3})$ profiles and $[\mathrm{O_3}]_{87}$ used. Although the uncertainties in the H and $\mathrm{O_3}$ profiles set limits on the accuracy of our derived H concentrations, in view of the paucity of other measurements of this constituent, we believe that our results are worthy of discussion.

The results of the calculation are shown in Figure 6. Each point plotted corresponds to a nocturnal mean [H] value, and the solid line shows the monthly averaged values. A strong seasonal variation can be seen, with maxima in July and December-January and minima in April and October, varing from 2.7×10^8 to 6.9×10^8, corresponding to a variation of approximately ±50% about the annual mean. As expected from (19), the [H] variation is in antiphase with that of $[\mathrm{O_3}]$.

The observed seasonal variations are in good agreement, not only in phase but also in amplitude, with *Thomas's* [1990b] data obtained from the SME satellite. Our data show, however, absolute atomic hydrogen concentrations about a factor of 3 greater than those obtained from the satellite measurements. Our results are also in reasonable agreement with the model calculation of *Le Texier et al.* [1987]. We conclude that our analysis of the simultaneous airglow and lidar observations indicates that the hydrogen concentration is controlled by vertical transport processes from the lower atmosphere as suggested by *Garcia and Solomon* [1985].

Uncertainties. The derived ozone and atomic hydrogen concentrations in the present work depend on the parameters used in (13) and (17). In Table 2 the range of uncertainty for each parameter is shown. With respect to the fraction a for the $\mathrm{Na}(^2P)$ yield of the reaction $\mathrm{NaO} + \mathrm{O} \rightarrow \mathrm{Na}(^2P) + \mathrm{O_2}$, for example, reported values cover a range of more than 30, from less than 0.01 [*Plane and Husain*, 1986] to 0.3 [*Bates and Ojha*, 1980]. It is interesting to note that our results support the higher values, around 0.3, rather than the much lower value. Using *Thomas's* [1990a] 0.004 mbar ozone mixing ratios for 25°S, our results give a mean value of 0.27. In the case of (17), for the hydrogen concentration, the main errors are in the values adopted for A_{94}/A_9, $f(9)$ and $k_{6,\mathrm{O_2}}/A_9$. In our analysis we have used the A_{94}/A_9 value of 4.84×10^{-3}, presented by *Murphy* [1971], which is in good agreement with observations [*Takahashi and Batista*, 1981]. A more recent theoretical calculation by *Turnbull and Lowe* [1989], however, suggests a much higher value of 1.47×10^{-2}. Consequently, the range of pos-

TABLE 3. Nighttime Sodium, Ozone and Hydrogen Density Profiles Adopted in This Study

	Peak Height, km	Maximum Density cm^{-3}	Source	Reference
Na	93	3600	lidar	*Simonich et al.*[1979]
$\mathrm{O_3}$	86	1.0×10^8	model	*Allen et al.*[1984]
$\mathrm{O_3}$	85	3.0×10^8	model	*Moreels et al.*[1977]
$\mathrm{O_3}$	92	5.8×10^8	rocket	*Vaughan*[1982]
$\mathrm{O_3}$	89	6.0×10^8	rocket	*Ulwick et al.* [1987]
H	83	2.9×10^8	model	*Allen et al.* [1984]
H	83	1.9×10^8	model	*Moreels et al.* [1977]
H	85	1.5×10^8	rocket	*Sharp and Kita* [1987]

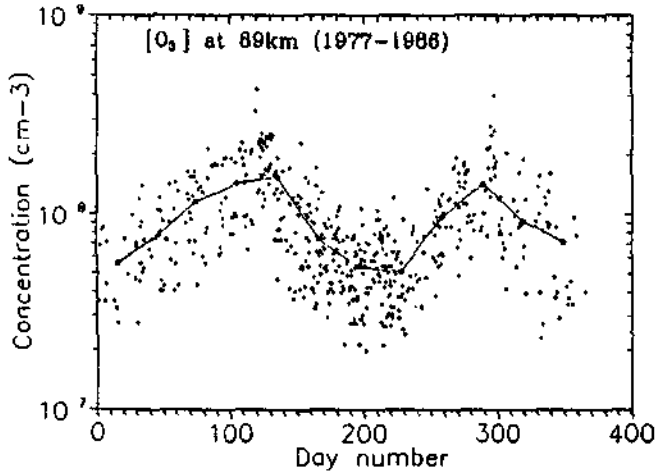

Fig. 5. Ozone concentrations at 89 km of altitude derived from the sodium atom and the sodium nightglow data as a function of the day number.

sible values for $k_{6,O_2}/A_9$ is from 5.3×10^{-14} [*McDade et al.*, 1987] to 1.4×10^{-13} (using *Turnbull and Lowe's* [1989] A_9 value). Values for $f(9)$ range from 0.3 [*Ohoyama et al.*, 1985] to 0.6 [*Llewellyn at al.*, 1978]. Therefore, the three parameters used in (17) contribute a total uncertainty of a factor of 3. With respect to the absolute values for the derived minor constituent concentrations, then, the error range is large. This does not apply, however, to the day-to-day and seasonal variations.

Regarding the day-to-day and seasonal variations of the hydrogen and ozone concentrations, the errors come mainly from temporal variations of the adopted height profiles, i.e., $p(\mathrm{Na})$, $p(\mathrm{O_3})$ and $p(\mathrm{H})$. The ozone profile observed by *Thomas* [1990a] indicates some variation with season. The range of variation of the profile was, however, less than the variability of the ozone profiles adopted in calculating (14). No information is available on the relative change in the hydrogen profile. Presently available hydrogen profiles listed in Table 3 were used to determine the maximum range of variation. Concerning the day-to-day variation of the Na profile, *Simonich et al.* [1979] reported very small height variations. In the present study, we checked the variation by using 35 days of data, each with more than 12 hours of continuous measurement. The standard deviation from the mean centroid height was ±1 km. An analysis of the monthly mean vertical distribution of sodium shows little seasonal variation in the height distribution, except for a consistent lowering of the centroid height by about 1 km in November. The error range in the $p(\mathrm{Na})$ of about ±1 km would cause an error in (14) of 1.3. This is smaller than that which originates from the uncertainty of the O_3 profile.

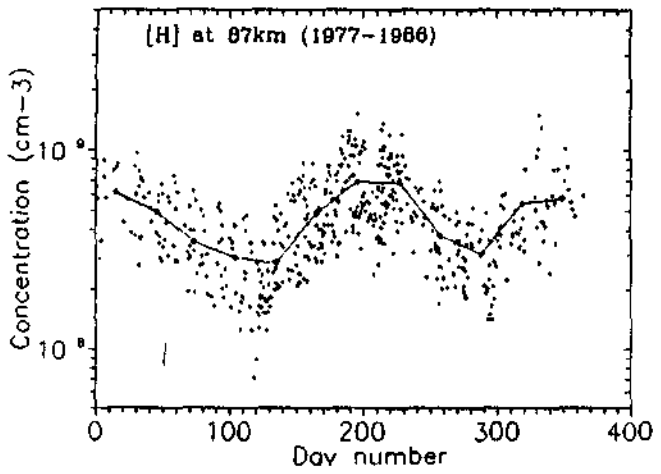

Fig. 6. Same as Figure 5, but for the hydrogen concentration.

The effect of the atmospheric temperature variations with season on the calculations of the H and O_3 concentrations should not be significant. According to *Clemesha et al.* [1990], the mesopause temperature at our latitude shows a small semiannual oscillation with equinox maxima, with an amplitude not more than 5 K. This would introduce error ranges of 3% in $[O_3]_{89}$ in (13) and 6% in $[H]_{87}$ in (17), owing to the temperature dependence of the reaction rates k_1 and k_5, respectively. On this basis it is concluded that the error range of approximately 20%, shown in (14) and (18), represents the range of uncertainty in the seasonal variation of the ozone and hydrogen concentrations in this study.

5. CONCLUSIONS

Seasonal variations of the mesospheric airglow emissions, OI5577, NaD and OH(9,4) band observed at Cachoeira Paulista (22.7°S, 45.0°W) were investigated using a long set of data from 1977 to 1986. The OI5577 and NaD emissions have strong semiannual variations, with maxima in April and October. The OH emission, on the other hand, showed less variation and its annual and semiannual components have almost the same amplitude. These results indicate that the atomic oxygen concentration at around 95 km has a strong semiannual variation. It is interesting to note, however, that the seasonal variation changes rapidly with height, and become very small in the OH emission region below 90 km.

The ozone concentration was derived from the NaD intensity and Na atom concentration observed by lidar. The hydrogen concentration was calculated by using the derived ozone and the OH(9,4) band intensity. The derived ozone concentration showed a strong semiannual variation, with maxima in April and October, its concentration varying between 5.4×10^7 and 1.5×10^8 cm^{-3}. The hydrogen concentration varies in antiphase with ozone, showing maxima in winter and summer. These results agree well with those reported by *Thomas* [1990a,b] from SME satellite data, and the model calculation by *Le Texier et al.* [1987].

The evidence for strong seasonal variations of the atomic oxygen, ozone and hydrogen concentrations in the mesopause region implies a seasonal variation in vertical transport processes. Increased gravity wave induced eddy transport at the solstices leads to more rapid transport of hydrogen compounds from the lower atmosphere. The resulting increase in atomic hydrogen leads to more rapid removal of atomic oxygen below 85 km, where the chemical lifetime for this species is small compared to the dynamical time constant. During the equinoxes, on the other hand, reduced eddy transport results in larger vertical gradients in O and H, with the result that the concentration of atomic oxygen increases above 90 km, but, as a result of the reduced H concentration, changes little in the region of 87 km where the OH emission is produced.

The present results show that simultaneous measurements of the mesospheric airglow emissions, together with Na lidar observations, constitute a useful technique for obtaining ozone and atomic hydrogen concentrations in the mesopause region.

Acknowledgments. The authors are grateful to the staff of the Cachoeira Paulista Airglow Observatory, Helio Borges and Pedro Paulo S. Braga for operating the photometers, and to Nelson R. Teixeira for data processing and analysis. This work was partly supported by the Fundo Nacional de Desenvolvimento Científico e Tecnológico (FNDCT) under contract FINEP-537/CT.

REFERENCES

Allen, M., J. I. Lunine, and Y. L. Yung, The vertical distribution of ozone in the mesosphere and lower thermosphere, *J. Geophys. Res., 89*, 4841-4872, 1984.

Baker, D. J., and A. T. Stair,Jr., Rocket measurements of the altitude distributions of the hydroxyl airglow, *Phys. Scr. 37*, 611-622, 1988.

Bates, D. R., Excitation of 557.7 nm OI line in nightglow, *Planet. Space Sci., 36*, 883-889, 1988.

Bates, D. R., and M. Nicolet, The photochemistry of atmospheric water vapor, *J. Geophys. Res., 55*, 301-327, 1950.

Bates, D. R., and P. C. Ojha, Excitation of the Na D doublet of the nightglow, *Nature, 286*, 790-791, 1980.

Clemesha, B. R., H. Takahashi, and P. P. Batista, Mesopause temperatures at 23°S, *J. Geophys. Res., 95*, 7677-7681, 1990.

Cogger, L. L., R. D. Elphinstone, and J. S. Murphree, Temporal and latitudinal 5577 Å airglow variations, *Can. J. Phys., 59*, 1296-1307, 1981.

Dickinson, P. H. G., W. C. Bain, L. Thomas, E. R. Williams, D. B. Jenkins, and N. D. Twiddy, The determination of the atomic oxygen concentration and associated parameters in the lower ionosphere, *Proc. R. Soc. London, Ser. A, 369*, 379-408, 1980.

Garcia, R. R., and S. Solomon, The effect of breaking gravity waves on the dynamics and chemical composition of the mesosphere and lower thermosphere, *J. Geophys. Res., 90*, 3850-3868, 1985.

Good, R. E., Determination of atomic oxygen density from rocket borne measurement of hydroxyl airglow, *Planet. Space Sci., 24*, 389-395, 1976.

Greer, R. G., and G. T. Best, A rocket-borne photometric investigation of the oxygen lines at 5577 Å and 6300 Å, the NaD lines and the continuum at 5300 Å in the night airglow, *Planet. Space Sci., 15*, 1857-1881, 1967.

Hedin, A. E., MSIS-86 Thermospheric model, *J. Geophys. Res., 92*, 4649-4662, 1987.

Keyser, L. F., Absolute rate and temperature dependence of the reaction between hydrogen(^{2}S) atoms and ozone, *J. Phys. Chem., 83*, 645-668, 1979.

Kirchhoff, V. W. J. H., B. R. Clemesha, and D. M. Simonich, Seasonal variation of ozone in the mesosphere, *J. Geophys. Res., 86*, 1463-1466, 1981.

Le Texier, H., S. Solomon, and R. R. Garcia, Seasonal variability of the OH Meinel bands,*Planet. Space Sci., 35*, 977-989, 1987.

Llewellyn, E. J. , B. H. Long, and B. H. Solheim, The quenching of OH* in the atmosphere, *Planet. Space Sci., 26*, 525-531, 1978.

McDade, I. C., D. P. Murtagh, R. G. H. Greer, P. H. G. Dickinson, G. Witt, J. Stegman, E. J. Llewellyn, L. Thomas, and D. B. Jenkins, ETON 2: Quenching parameters for the proposed precursors of $O_2(b^1\sum_g^+)$ and O(^{1}S) in the terrestrial nightglow, *Planet. Space Sci., 34*, 789-800, 1986.

McDade, I. C., E. J. Llewellyn, D. P. Murtagh, and R. G. H. Greer, ETON 5: Simultaneous rocket measurements of the OH Meinel v=2 sequence and (8,3) band emission profiles in the nightglow, *Planet. Space Sci., 35*, 1137-1147, 1987.

Moreels, G., G. Megie, A. Vallance Jones, and R. L. Gattinger, An oxygen-hydrogen atmospheric model and its application to the OH emission problem, *J. Atmos. Terr. Phys., 39*, 551-570, 1977.

Murphy, R. E., Infrared emission of OH in the fundamental and first overtone bands, *J. Chem. Phys., 54*, 4852-4859, 1971.

Murtagh, D. P., G. Witt, J. Stegman, I. C. McDade, E. J. Llewellyn, F. Harris, and R. G. H. Greer, An assessment of proposed O(^{1}S) and $O_2(b^1\sum_g^+)$ nightglow excitation parameters, *Planet. Space Sci., 38*, 43-53, 1990.

Ohoyama, H., T. Kasai, Y. Yoshimura, H. Kimura, and K. Kuwata, Initial distribution of vibration of the OH radicals produced in the H + O_3 → OH($X^2\Pi$) + O_2 reaction, *Chem. Phys. Lett., 118*, 263-266, 1985.

Plane, J. M. C., and D. Husain, Determination of the absolute rate constant for the reaction O + NaO → Na + O_2 by time-resolved atomic chemiluminescence at λ = 589 nm [Na(3^2P_J) → Na($3^2S_{1/2}$)+$h\nu$], *J. Chem. Soc. Faraday Trans. 2, 82*, 2047-2052, 1986.

Rodrigo, R., J. J. Lopez-Moreno, M. Lopez-Puertas, and A. Molina, Analysis of OI-557.7 nm, NaD, OH(6-2) and $O_2(b^1\sum_g^+)$(0-1) nightglow emissions from ground-based observations, *J. Atmos. Terr. Phys.,47*, 1099-1110, 1985.

Sharp, W. E., and D. Kita, In situ measurement of atomic hydrogen in the upper mesosphere, *J. Geophys. Res., 92*, 4319-4324, 1987.

Simonich, D. M., B. R. Clemesha, and V. W. J. H. Kirchhoff, The mesospheric sodium layer at 23°S: Nocturnal and seasonal variations, *J.Geophys. Res., 84*, 1543-1550, 1979.

Stegman, J., and G. Witt, Rocket-borne sodium nightglow measurement during post-auroral conditions, *Space Res., 17*, 287-290, 1977.

Takahashi, H., and P. P. Batista, Simultaneous measurements of OH(9,4), (8,3), (7,2), (6,2), and (5,1) bands in the airglow, *J. Geophys. Res., 86*, 5632-5642, 1981.

Takahashi, H., P. P. Batista, B. R. Clemesha, D. M. Simonich, and Y. Sahai, Correlations between OH, NaD and OI 5577 Å emissions in the airglow, *Planet. Space Sci., 27*, 801-807, 1979.

Takahashi, H., Y. Sahai, and P. P. Batista, Tidal and solar cycle effects on the OI 5577 Å, NaD and OH(8,3) airglow emissions observed at 23°S, *Planet Space Sci., 32*, 897-902, 1984.

Takeuchi, I., K. Misawa, Y. Kato, and I. Aoyama, Seasonal variations of the correlation among nightglow radiations and emission mechanism of OH nightglow emission, *J. Atmos. Terr. Phys., 43*, 157-164, 1981.

Thomas, R. J., Seasonal ozone variations in the upper mesosphere, *J. Geophys. Res. 95*, 7395-7401, 1990a.

Thomas R. J., Atomic hydrogen and atomic oxygen density in the mesopause region: Global and seasonal variations deduced from Solar Mesosphere Explorer near-infrared emissions, *J. Geophys. Res., 95*, 16457-16476, 1990b.

Turnbull, D. N., and R. P. Lowe, New hydroxyl transition probabilities and their importance in airglow studies, *Planet. Space Sci., 37*, 723-738, 1989.

Ulwick, J. C., K. D. Baker, D. J. Baker, A. J. Steed, W. R. Pendleton, Jr., K. Grossmann, and H. G. Bruckelmann, Mesospheric minor species determinations from rocket and ground-based i.r. measurements, *J. Atmos. Terr. Phys., 49*, 855-862, 1987.

Vaughan, G., Diurnal variation of mesospheric ozone, *Nature, 296*, 133-135, 1982.

Wiens, R. H., and G. Weill, Diurnal, annual and solar cycle variations of hydroxyl and sodium nightglow intensities in the Europe-Africa sector, *Planet. Space Sci., 21*, 1011-1027, 1973.

Witt, G., J. Stegman, B. H. Solheim, and E. J. Llewellyn, A measurement of the $O_2(b^1\sum_g^+ - X^3\sum_g^-)$ atmospheric band and the OI(^{1}S) green line in the nightglow, *Planet. Space Sci., 27*, 341-350, 1979.

Worsnop, D. R., M. S. Zahniser, and C. E. Kolb, Low temperature absolute rate constants for the reaction of atomic sodium with ozone and nitrous oxide, *J. Phys. Chem., 95*, 3960-3964, 1991.

P. P. Batista, B. R. Clemesha, Y. Sahai, D. M. Simonich, and H. Takahashi, Instituto Nacional de Pesquisas Espaciais (INPE), CP 515, 12201, São José dos Campos, SP, Brazil.

(Received June 17, 1991;
revised December 3, 1991;
accepted December 3,1991.)